Gas-liquid Taylor flow in microchannels

T. Abadie[a,b], J. Aubin[b], D. Legendre[a], C. Xuereb[b]

a. *Institut de Mécanique des Fluides, 1 Allée du Professeur Camille Soula, 31400 TOULOUSE*
b. *Laboratoire de Génie Chimique, 4 Allée Emise Monso, BP 84-234, 31432 TOULOUSE*

Résumé :

Cette étude, comportant un volet expérimental et un volet numérique, vise à mieux comprendre l'hydrodynamique des écoulements de Taylor gaz-liquide en microcanaux rectangulaires ($d_h \sim 500\,\mu m$). L'étape de génération des bulles lors de la mise en contact des fluides est étudiée expérimentalement à travers la taille des bulles et bouchons liquide en fonction des propriétés des fluides et des conditions opératoires. Les résultats sont confrontés à une corrélation dépendant uniquement de la géométrie et du rapport de débit gaz/liquide. Il est mis en évidence que l'influence des propriétés des fluides et des conditions opératoires n'est pas négligeable dans nos expériences. La forme des bulles, ainsi que la quantité de liquide autour de la bulle de Taylor dans l'écoulement établi sont également analysées à partir des simulations numériques basées sur une méthode 'Volume Of Fluid'.

Abstract :

This study, which comprises an experimental and a computational approach, aims at improving the understanding of gas-liquid Taylor flow in rectangular microchannels ($d_h \sim 500\,\mu m$). The bubble generation mechanism at the fluids contacting is studied experimentally through bubble and slug lengths depending on fluid properties and operating conditions. The results are compared with a correlation where bubble lengths only depend on geometry and ratio of gas over liquid flow rates. It has been observed that the effects of fluid properties and operating conditions cannot be neglected in our experiments. The bubble shapes, as well as liquid film hold-up in the established Taylor flow are also analysed from the numerical simulations based on the Volume Of Fluid method.

Key words : Taylor bubble ; experimental visualisations ; numerical simulations

1 Introduction

Microreactors are particularly interesting for fast highly exothermic and/or mass transfer limited gas-liquid reactions since heat and mass transfer is remarkably intensified. Slug or Taylor flow is the flow configuration that occurs for a large range of flow conditions [1]. Taylor flow is characterised by regular sized bubbles that are longer than the microchannel width or diameter and separated by slugs of liquid. The bubbles fill almost all the entire cross-section of the channel and are separated from the wall by a thin liquid layer. Taylor flow in microreactors is an interesting flow regime because it intensifies both mass and heat transfer due to the fluid recirculation generated in the liquid slug [8]. However, controlling the flow regime and the characteristic size of the gas-liquid dispersion remains a difficult task. The present work aims at improving the fundamental understanding of gas-liquid Taylor flow in microchannels. In particular, the objective of this study is to investigate the effects of the physical properties of the fluids and the flow rates on the characteristics of the gas-liquid dispersion generated in a T-junction microchannel. Visualisation experiments and direct numerical simulations have been performed in order to obtain information on the bubble generation mechanism, bubble velocity, bubble and slug lengths, as well as the liquid film surrounding the bubble body.

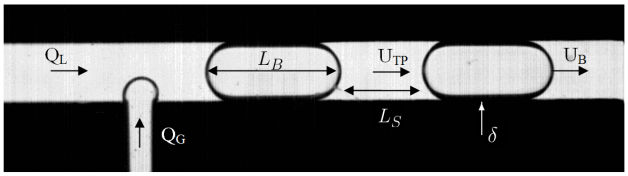

Figure 1: Contacting section: bubble formation. The notations used are: $Q_{G,L}$ for gas and liquid flow rates, $L_{B,S}$ for bubble and slug lengths, δ the liquid film thickness, U_B the bubble velocity and U_{TP} the superficial two-phase velocity ($U_{TP} = (Q_L + Q_G)/A_{ch} = U_L + U_G$). A_{ch} is the cross section area.

2 Experimental set-up

2.1 Microchannel characteristics & Flow control equipment

Rectangular cross-section microchannels have been etched through a silicon wafer plate using Deep Reactive Ionic Etching (DRIE) technique, sandwiched between glass wafers and bonded using anodic bonding. The gas and liquid are contacted using a side-entering T-junction as shown in Figure 2 and the main channel has a meandering topology with curved bends. Liquid is flowing in the main channel while the gas is supplied perpendicularly via a narrower channel. The hydraulic diameter is $d_h = 571\,\mu m$ and the aspect ratio $w/h = 2.5$ (see Figure 2 for the overall dimensions).

Figure 2: Contacting section: side entering T-junction, channel geometry: meandering microchannel with $w_{l,in} = 1\,mm = w$, $w_{g,in} = 525\,\mu m$, $h = 400\,\mu m$, $d_h = 571\,\mu m$, $l \sim 30\,cm$

Bubble lengths and velocities have been studied with a general liquid-gas system [11]. The gas (air in all the experiments) is supplied from a pressurized vessel and controlled by a mass-flow controller which allows volumetric flow rates ranging from 0.00 to $1.00\,mL/min$. Liquid flow is controlled using a syringe pump which allows flow rates ranging from 0.000 to $1.000\,mL/min$. All the experiments were conducted under room temperature and ambient pressure. The images have been recorded with a high-speed camera ($462 fps$ at full resolution $1024 \times 1024\ pix^2$) and a shutter time short enough to obtain a distinct gas-liquid interface ($\sim 1\,ms$). Bubble and slug lengths, such as velocities were evaluated following the interface with an image processing software for every bubble entering the observation window and averaged within a representative sample.

2.2 Operating conditions

The fluid system we started with is an ethanol-air system which allows a regular and relatively easy bubble formation [11]. Then, the effects of surface tension on bubble generation and hydrodynamics have been studied using water and ethanol/water solutions. Table 1 summarises the ranges of velocities and dimensionless numbers explored in the experiments. The values of the capillary numbers (viscosity/capillarity) and Weber numbers (inertia/capillarity) indicate that the main contribution in these flows is the capillary force. Thus, we can assume that the shape of the bubbles is mainly governed by capillarity. We can see with the Reynolds numbers that inertial term dominates viscous term. In addition, the Bond number (gravitational effects/capillarity) is less than unity ($Bo_{max} = 0.11$). Thus, surface tension dominate gravitational effects.

fluid	Q_L (mL/min)	Q_G (mL/min)	U_{LS} $(10^{-2}m/s)$	U_{GS} $(10^{-2}m/s)$	Re_{TP}	Ca_{TP} 10^{-3}	We_{TP} 10^{-2}	Bo
air-EtOH	0.2 - 1	0.04 - 1	0.83 - 4.2	0.17 - 4.2	4 - 32.9	0.52 - 4.35	0.21 - 14	0.115
air-EtOH (33%)	0.3 - 1	0.06 - 1	0.83 - 4.2	0.17 - 4.2	3.3 - 18.5	0.97 - 5.4	0.32 - 10	0.080
air-water	0.2 - 1	0.04 - 1	0.83 - 4.2	0.17 - 4.2	10.6 - 35.5	0.49 - 1.64	0.52 - 5.8	0.047

Table 1: Velocities and dimensionless numbers

3 Numerical simulations

3.1 Governing equations and numerical schemes

The numerical code used for this study is the JADIM code [6] developed to perform local analyses of dipersed two-phase flows. The interface capturing technique implemented in this code is the Volume of Fluid method (VOF) which consists in a Eulerian description of each phase on a fixed grid. Under the following assumptions: (i) Newtonian and incompressible fluids, (ii) no mass transfer at the interface, (iii) isothermal and (iv) constant surface tension, the fluid flow is described by the classical one fluid formulation of the Navier-Stokes equations :

$$\nabla \cdot \mathbf{U} = 0 \qquad and \qquad \rho \left(\frac{\partial \mathbf{U}}{\partial t} + (\mathbf{U} \cdot \nabla)\, \mathbf{U} \right) = -\nabla P + \nabla \cdot \mathbf{\Sigma} + \rho \mathbf{g} + \mathbf{F}_{\sigma,\mathbf{v}} \tag{1}$$

where $\mathbf{\Sigma}$ is the viscous stress tensor, $\mathbf{g}$ is the acceleration due to gravity. $\mathbf{F}_{\sigma,\mathbf{v}} = -\sigma \nabla \cdot \left(\frac{\nabla C}{\|\nabla C\|} \right) \nabla C$ is the capillary contribution where σ is the surface tension, the normal to the interface is the gradient of volume fraction, and the force is localized via a non zero volume fraction gradient. ρ and μ are the local density and dynamic viscosity. They are deduced from the volume fraction C of one phase by a linear interpolation : $\rho = C\,\rho_1 + (1 - C)\,\rho_2$ and $\mu = C\,\mu_1 + (1 - C)\,\mu_2$, where the volume fraction is $C = 1$ (resp. $C = 0$) in cells filled with fluid 1 (resp. fluid 2) and $0 < C < 1$ in cells cut by the interface. An additional transport equation of the volume fraction of one phase (or color function), is solved to capture the interface between the two phases:

$$\frac{\partial C}{\partial t} + \mathbf{U} \cdot \nabla C = 0 \tag{2}$$

In many VOF methods employed to capture the interface, a reconstruction technique step is used to control the thickness of the interface. In JADIM, the interface location and thickness are both controlled by an accurate algorithm based on Flux-Corrected Transport schemes. The equations are discretized on a staggered grid using a finite volume method, all spatial derivatives being approximated using second-order centered schemes. The time scheme used to compute the advective terms in the Navier-Stokes equations is a third-order Runge-Kutta type scheme, while viscous stresses are solved using a semi-implicit Crank-Nicolson method. The incompressibility is ensured with a projection method, which consists in parsing the velocity field into two contributions : a rotational one, which gives a predicted velocity field calculated semi-implicitely, and a potential one, obtained from a pressure correction solution of a pseudo-Poisson equation, whose divergence is null.

The capillary contribution $\mathbf{F}_{\sigma,\mathbf{v}}$ is of main importance in flows controlled by capillarity as observed in microchannels. The numerical method used to solve the interfacial force is the Continuum Surface Force (CSF) proposed by Brackbill *et al.* [4]. The discretization of the capillary force is well known to produce artificial vorticity in the vicinity of the interface and unphysical streams called 'spurious currents' ([4],[6]). In the case of a static cylindrical drop at equilibrium, it appeared that the maximum velocity is $u_{SC} \sim 0.01\frac{\sigma}{\mu}$ that leads to a critical capillary number $Ca_{SC} \sim 0.01$ [6]. Below this capillary number Ca_{SC}, the spurious currents are non negligible. The fluid properties were chosen so that spurious currents are negligible compared with bubble velocity.

3.2 Mesh and boundary conditions

2D numerical simulations which simulate a channel infinitely wide were performed in a dimensionless plane ($l_x^* \times l_y^* = 17 \times 1$) to simulate half a height of the channel. In these 2D geometries, the lateral

wall effects are not taken into account even if it is known that liquid flows from the corner to the center of the channel and can have effects on the flow properties such as the liquid film thickness or bubble shape. A pressure gradient is imposed between two periodic boundary conditions to generate motion. Two meshes were used to correctly capture the liquid film surrounding the bubble depending on the shape of the bubble since about 5 cells are needed in the liquid film [8] : a first mesh which comprises 15300 cells with a uniform grid spacing ($n_x \times n_y = 510 \times 30$) ; and a second one which comprises 7620 cells, refined close to the wall with a factor 0.92 in the y direction ($n_x \times n_y = 254_{\times}30$).

4 Gas-liquid dispersion

4.1 Bubble generation, Bubble and Slug lengths

Figure 3 shows the bubble generation mechanism for the ethanol-air system. This mechanism can be partitioned into several steps: (a to b) the bubble starts growing perpendicularly to the direction of the liquid flow in the main channel; (b to d) as the bubble grows, the gas-liquid interface is distorted by the liquid in the main channel; (d) during this time, the interface detaches from the upstream wall of the gas inlet and the contact line starts moving into the gas inlet; (d to e) the air fills the main channel; (e to f) the gas-liquid interface coming from the gas inlet is pushed downstream until pinching off occurs and the bubble is formed.

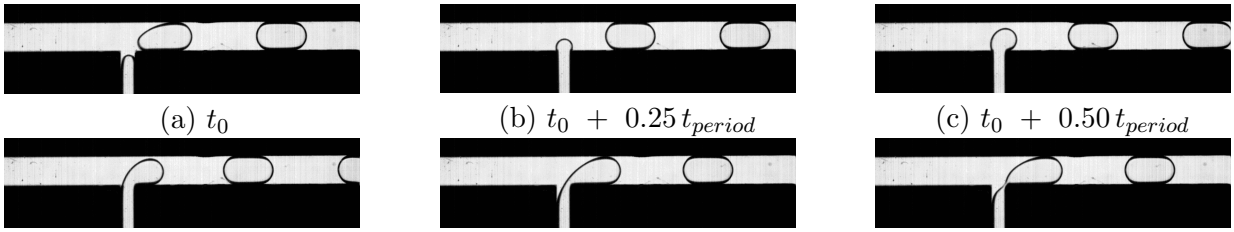

(a) t_0 (b) $t_0 + 0.25\,t_{period}$ (c) $t_0 + 0.50\,t_{period}$

(d) $t_0 + 0.72\,t_{period}$ (e) $t_0 + 0.93\,t_{period}$ (f) $t_0 + 0.99\,t_{period}$

Figure 3: Bubble generation in ethanol-air flows. $U_L = 0.021\,m/s = 2 \times U_G$, Taylor flow during a period where bubbles are generated every $t_{period} = 0.125\,s$, *i.e.* with a formation frequency of $8Hz$

Estimating the characteristic times of each step, under the assumption that filling and squeezing stages are well uncoupled and the bubble occupies the entire cross section, a scaling law can be proposed to estimate the bubble lengths ([7],[9]). The slug length can be estimated the same way.

$$\frac{L_B}{w} = \lambda_1 + \lambda_2 \frac{Q_G}{Q_L} \qquad and \qquad \frac{L_S}{w} = \lambda_2 + \lambda_1 \frac{Q_L}{Q_G} \tag{3}$$

Since liquid flows in the corners of the channel during the bubble generation process, coefficients λ_1 and λ_2 are introduced instead of being unity [9]. In ethanol-air experiments, bubbles are generated following this mechanism and regular bubble trains are observed. However, when working with water, interface rupture occurs mainly in the main channel with a necking phenomenon after the junction due to an increased leakage flow around the bubble during generation. Figure 4.a. shows the bubble lengths versus the ratio of gas over liquid flow rates. For a given liquid velocity and increasing the gas velocity, bubbles are longer in water-air systems, than ethanol 33%-air and finally ethanol-air systems. The linear evolution of the bubble lengths with the flow rate ratios is in agreement with the model proposed by Garstecki *et al.* [7]. However, the coefficients in this linear scaling law appear to depend on operating conditions and fluid properties. The transition between short bubbles with a high frequency of break-up (like ethanol experiments) to longer bubbles with a low frequency of break-up (like water experiments) when decreasing the liquid velocity has been observed using ethanol 33%.

4.2 Bubble shapes, Liquid film hold-up

The liquid film surrounding the bubble has been studied for a long time since the first experiments of Taylor [10] in circular tubes and the theoretical study of Bretherton using the 'lubrication approximation' at low capillary numbers [5]. Aussillous & Quéré [2] extended this study to higher capillary

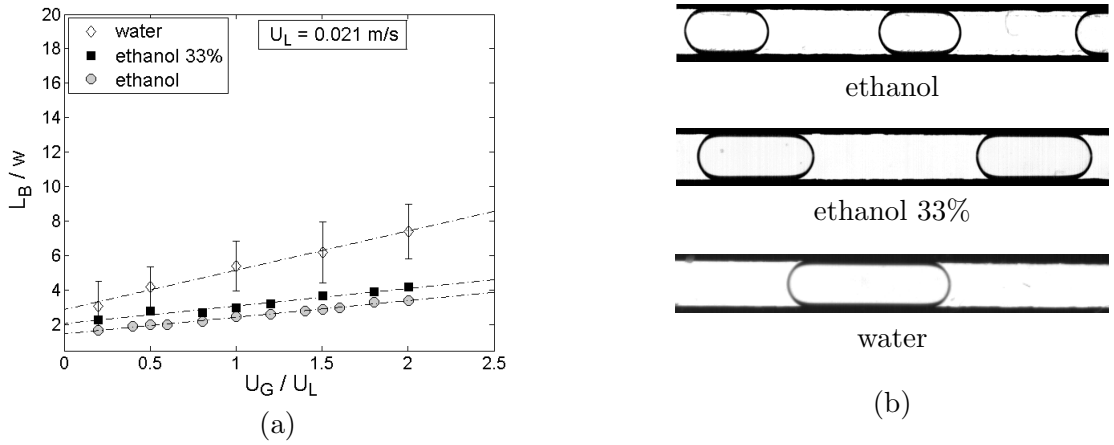

(a) (b)

Figure 4: (a) Dimensionless bubble lengths for varying gas phase velocities and a fixed liquid phase velocity $U_L = 0.021\,m/s$ for water, $We_L \sim 0.43$ ($\Diamond$), ethanol 33%, $We_L \sim 0.30$ ($\square$) and ethanol, $We_L \sim 0.18$ ($\circ$). Errorbars represent the standard deviation for the water-air system; the standard deviation on bubble lengths for the ethanol and the ethanol 33% systems was negligible. $-\cdot-$ experimental fitting. (b) Illustration of bubble trains for the three liquid-air systems for $U_L = 0.021\,m/s = 2{\times}U_G$

numbers to estimate liquid film thickness in capillary tubes. Since the measurement of liquid film hold-up in rectangular microchannels is not straightforward experimentally, the liquid film has been studied from 2D and axisymmetric numerical simulations to compare our results with [2] (Figure 5).

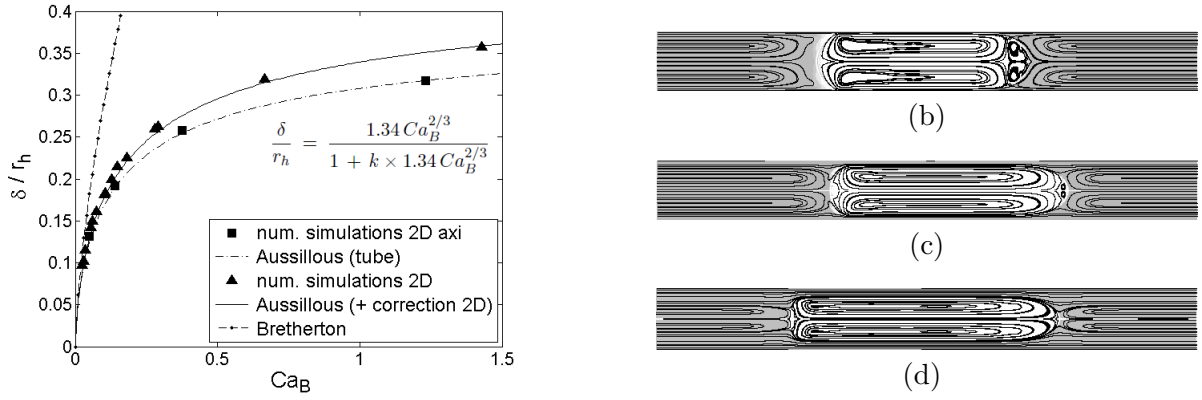

(a) (b) (c) (d)

Figure 5: (a) Liquid film thickness versus capillary number. 2D numerical simulations at (b) $Ca = 0.029$; (c) $Ca = 0.131$; (d) $Ca = 0.509$ and $Re = 5.6 \times Ca$.

The axisymmetric simulations agree very well with Aussillous & Quéré correlation (with coefficient $k \sim 2.5$) and the 2D simulations follow a similar scaling law (with $k \sim 2.2$). For a given capillary number, the liquid film is thicker in two dimensional channels. Under the assumption that the velocity is zero in the liquid film, which is verified in 2D and axisymmetric simulations, the bubble velocity can be related to the mean velocity in the slug using the mass conservation. In addition to the increase in the liquid film thickness, we can observe changes in the recirculation areas in both phases. Indeed, increasing the capillary number leads to a decrease in the size of the recirculation zone in the nose of the bubble until vanishing while the main recirculation in the bubble is elongated. In the slug, the center of the streamlines moves closer to the center of the channel when increasing the capillary number. The shape of the bubble also changes, we can observe an elongation of the front cap and a flattening of the rear of the bubble and even a change in the sign of the curvature at high capillary

numbers (about unity). These changes lead to a pressure drop decreased at the rear and increased at the front cap when capillary number increases. Thus, the pressure drop across the bubble increases with the capillary number. Experimentally, these phenomena (increase in the liquid film thickness and change in the shape of the bubble) have been observed qualitatively with ethanol-air systems. As expected, the bubble is symmetric at low capillary numbers and starts being distorted when capillary number increases. The capillary number is not the only parameter to take into account to characterize bubble shape. Inertia can also play an important role as mentioned by Aussillous & Quéré. It has been observed in numerical simulations by varying density and thus the Reynolds number.

5 Conclusions

This study has focused on the generation and characteristics of gas-liquid Taylor flow formed in T-junction microchannels. As earlier described by Garstecki *et al.* [7] and then Van Steijn *et al.* [9], the bubble generation process can be partitioned into several steps and the bubble and slug lengths are a function of gas and liquid flow rates and independant of fluid properties. However, it has been shown in this study that bubble and slug lengths do not depend solely on the fluids flow rates and suggest the liquid properties and velocity are also a parameter to take into account. It would be interesting to simulate computationally the generation process to control accurately fluids and wall properties. Bubble shapes and liquid film thickness have been studied computationally. The changes in the curvature and pressure drops at the bubble caps have been mentioned. The distortions due to inertia and viscous stresses are not well understood yet. Three dimensional simulations will be necessary for a more accurate characterization of the flow and a comparison with experiments.

Acknowledgements :

This work was financed by the french 'Agence Nationale de la Recherche' in the framework of the project MIGALI no. ANR-09-BLAN-0381-01. We also acknowledge the support for this project from the CNRS research federation FERMaT, and the CALMIP project for providing computational resources.

References

[1] Akbar, M.K., Plummer, D.A., Ghiaasiaan, S.M. 2003 On gas-liquid two-phase flow regimes in microchannels. *Int. J. of Multiphase Flow* **29** 855-865

[2] Aussillous, P., Quéré, D. 2000 Quick deposition of a fluid on the wall of a tube. *Phys. of Fluids* **12** (10), 2367

[4] Brackbill, J., Kothe, D.B., Zemach, C. 1992 A continuum method for modeling surface tension. *J. Comp. Phys.* **100** 335-354

[5] Bretherton, F.P. 1961 The motion of long bubbles in tubes. *J. Fluid Mech.* **10** 166

[6] Dupont, J-B., Legendre, D. 2010 Numerical simulation of static and sliding drop with contact angle hysteresis. *J. Comp. Phys.* **229** 2453-2478

[7] Garstecki, P., Fuerstman, M.J., Stone, H.A., Whitesides, G.M. 2006 Formation of droplets and bubbles in a microfluidic T-junction - scaling and mechanism of break-up. *Lab on a chip.* **6** 437-446

[8] Gupta, R., Fletcher, D.F., Haynes, B.S. 2009 On the CFD modelling of Taylor flow in microchannels. *Chem. Eng. Sc.* **64** 2941-2950

[9] van Steijn, V., Kreutzer, M.T., Kleijn, C.R. 2007 μ-PIV study of the formation of segmented flow in microfluidic T-junction. *Chem. Eng. Sc.* **62** 7505-7514

[10] Taylor, G.I. 1961 Deposition of a viscous fluid on the wall of a tube. *J. Fluid Mech.* **10** 161-165

[11] Volkel, N. 2009 Design and characterization of gas-liquid microreactors. *PhD. Thesis, Institut National Polytechnique de Toulouse, France*